Response and Discrimination Performance of Arrays of Organothiol-Capped Au Nanoparticle Chemiresistive Vapor Sensors

ARTICLE *in* THE JOURNAL OF PHYSICAL CHEMISTRY C · MARCH 2011

Impact Factor: 4.77 · DOI: 10.1021/jp110793h

6 AUTHORS, INCLUDING:

Edgardo García-Berríos
KLA-Tencor
10 PUBLICATIONS **92** CITATIONS

SEE PROFILE

Bruce Brunschwig
California Institute of Technology
202 PUBLICATIONS **7,685** CITATIONS

SEE PROFILE

THE JOURNAL OF PHYSICAL CHEMISTRY C

ARTICLE

pubs.acs.org/JPCC

Response and Discrimination Performance of Arrays of Organothiol-Capped Au Nanoparticle Chemiresistive Vapor Sensors

Edgardo García-Berríos,[†] Ting Gao,[‡] Jordan C. Theriot,[†] Marc D. Woodka,[†] Bruce S. Brunschwig,[§] and Nathan S. Lewis*[,†,§]

[†]Division of Chemistry and Chemical Engineering, California Institute of Technology, 210 Noyes Laboratory, 127-72, Pasadena, California 91125, United States

[‡]Polymer, Ceramics, Technical Services Laboratories, Tyco Electronics Corporation, 306 Constitution Drive, Menlo Park, California 94025, United States

[§]Beckman Institute, California Institute of Technology, Pasadena, California 91125, United States

Supporting Information

ABSTRACT: The response and discrimination performance of an array that consisted of 20 different organothiol-capped Au nanoparticle chemiresistive vapor sensors was evaluated during exposure to 13 different organic vapors. The passivating organothiol ligand library consisted of collections of straight-chain alkanethiols, branched alkanethiols, and aromatic thiols. A fourth collection of sensors was formed from composites of 2-phenylethanethiol-capped Au nanoparticles and nonpolymeric aromatic materials that were coembedded in a sensor film. The organic vapors consisted of six hydrocarbons (*n*-hexane, *n*-heptane, *n*-octane, isooctane, cyclohexane, and toluene), three polar aprotic vapors (chloroform, tetrahydrofuran, and ethyl acetate), and four alcohols (methanol, ethanol, isopropanol, and 1-butanol). Trends in the resistance response of the sensors were consistent with expected trends in sorption due to the properties of the test vapor and the molecular structure of the passivating ligands in the sensor films. Classification algorithms including principal components analysis and Fisher's linear discriminant were used to evaluate the discrimination performance of an array of such sensors. Each collection of sensors produced accurate classification of most vapors, with misclassification occurring primarily for vapors that had mutually similar polarity. The classification performance for an array that contained all of the sensor collections produced nearly perfect discrimination for all vapors studied. The dependence of the array size (i.e., the number of sensors) and the array chemical diversity on the discrimination performance indicated that, for an array of 20 sensors, an array size of 13 sensors or more produced the maximum discrimination performance.

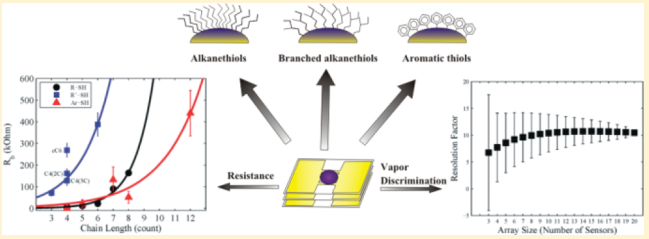

I. INTRODUCTION

An array of broadly cross-reactive sensors, in which each individual sensor responds to a variety of odors, is known as an electronic nose. Patterns of responses across the array produce a fingerprint for each odorant. Pattern recognition algorithms can then be employed to obtain information on the polarity and/or physicochemical properties, and concentration, of the vapor(s) exposed to the sensor array.[1−4]

Sensor arrays in which each individual sensor contains a unique functional group have attracted interest because of the ability of such arrays to classify organic and inorganic vapors.[5−7] In one approach, the functional group can be varied in polymers that are combined with a percolative network of carbon black (CB).[8,9] Another approach involves the use of an array of nonpolymeric organic materials (NPOM) as the organic sorption phase in composites with CB.[5] In these systems, sorption of an analyte effects a swelling of the organic phase, producing an increase in the resistance of the CB composite sensor film.

Films of Au nanoparticles (Au-NPs) capped with organothiol ligands have also been investigated as chemical vapor sensors.[10−13] Organically capped metal nanoparticles consist of a small metal core (typically less than 10 nm in diameter) surrounded by a dense organic layer of insulating material that is used to chemically passivate the metal particles. These materials, with a stoichiometry of ∼3:1 (Au:S-R), are easily synthesized using wet chemical techniques, and can remain soluble and chemically stable for extended periods in common organic solvents.[14−16] When exposed to a vapor, each Au-NP sensor film in the array will swell due to sorption of the analyte vapor. Sorption of vapor into Au-NP films produces either an increase or a decrease in film resistance upon exposure to analyte vapors.[12,13,17−19] This sensing mechanism thus allows exploitation of a unique capability of the Au-NP materials relative to other materials such

Received: November 11, 2010
Revised: January 6, 2011
Published: March 15, 2011

as polymer/CB sensors. The ability to control the direction of the sensor resistance response could significantly increase the ability of such an array to identify or classify vapors. Ibañez et al. observed decreases in resistance when a film composed of tetraoctylammonium bromide (TOABr)-functionalized Au-NPs was exposed to methanol, ethanol, isopropanol, or toluene.[19] The ability to control the sign of the sensor response to an analyte by use of different phase-transfer reagents could also add unique capabilities to arrays of such sensors. Han et al. and Wang et al. showed that arrays composed of a series of carboxylate-terminated ligands, dithiol ligands, and 1-decanethiol ligands, that had been embedded in the same matrix, could discriminate between *n*-hexane, benzene, toluene, and other nitroaromatic compounds, at a variety of concentrations, by use of principal components analysis (PCA) or by use of artificial neural networks.[20−22]

In this work, the response and the discrimination performance of four groups of organothiol-capped Au-NPs sensor arrays has been evaluated in response to a variety of test vapors. The sensitivity values have been correlated to the molecular structure of the passivating ligand, to elucidate the response mechanism of the sensor films. The first group of film compositions consisted of Au-NPs capped with straight-chain alkanethiols (R-SH), the second group consisted of Au-NPs capped with branched alkanethiols (R′-SH), and the third group consisted of Au-NPs capped with aromatic ligands (Ar-SH). The fourth group consisted of NPOM/Au-NP composite sensors formed by mixing with the NPOM passivated Au-NPs that contained a ligand with a terminated functional group that would have a homogeneous molecular interaction, with the NPOM. Such Au-NPs were capped with 2-phenylethanethiol mixed with aromatic molecules, to produce a film that was composed of 25% organic matrix and 75% Au by mass (C2Ph(Ar)). The library of analytes studied herein expands the number of analyte vapors that can be classified by Au-NPs sensor arrays. The analytes were chosen to have similar physicochemical properties, because vapor classification becomes more difficult as the vapor properties become increasingly mutually similar. The library of tested analyte vapors included six hydrocarbons (*n*-hexane, *n*-heptane, *n*-octane, isooctane, cyclohexane, and toluene), three polar aprotic vapors (chloroform, tetrahydrofuran, and ethyl acetate), and four alcohols (methanol, ethanol, isopropanol, and 1-butanol). The discrimination performance analysis involved the evaluation of the ability of each sensor array group to classify the test chemical vapors. The discrimination performance of an array that included all of the sensors investigated herein was also studied. Vapor discrimination was also evaluated as a function of the array size (i.e., number of sensors) and the average sensitivity of the array. The discrimination analysis was explored using PCA to visualize the array response clustering, and using Fisher's linear discriminant (FLD) to determine the resolution factor of binary combination of analyte responses. FLD was also used to quantify the cluster separation and the overlapping of responses between different analytes when PCA projections were used.

II. EXPERIMENTAL SECTION

A. Materials. Lithium aluminum hydride (95%), sodium borohydride (98%), hydrogen tetrachloroaurate trihydrate ($HAuCl_4 \cdot 3H_2O$, ≥ 99.9%), tetraoctylammonium bromide (≥99%), 1-butanethiol (99%), 1-pentanethiol (98%), 1-heptanethiol (98%), 1-octanethiol (98.5%), 2-methyl-1-propanethiol (92%), 2-methyl-1-butanethiol (97%), 3-methyl-1-butanethiol (95%), cyclohexanethiol (97%), 2-ethylhexanethiol (97%), benzenethiol (98%), 2-naphthalenethiol (99%), 4-biphenylsulfonyl chloride, 2-anthracenesulfonyl chloride (90%), 1,1′,4′,1″-terphenyl-4-thiol (97%), naphthalene (99%), biphenyl (99%), anthracene (99%), and *p*-terphenyl (99%), and the test analytes *n*-hexane (Hex), *n*-heptane (Hept), *n*-octane (Oct), isooctane (*i*Oct), and cyclohexane (*c*Hex) were obtained from Sigma-Aldrich. Toluene (Tol), chloroform (Chl), tetrahydrofuran (THF), ethyl acetate (EtOAc), methanol (MeOH), ethanol (EtOH), isopropanol (*i*POH) and 1-butanol (BuOH) were obtained from EM Science and 1-hexanethiol (97%) was obtained from Alfa Aesar. All of the reagents and solvents were used without further purification. Deionized water with 18 MΩ·cm resistivity was obtained from a Barnstead Nanopure purification system.

The synthesis of 4-biphenylthiol and 2-anthracenethiol was performed by the reduction of the sulfonyl chloride with lithium aluminum hydride, followed by the addition of diluted hydrochloric acid.[23−25] Characterization of these ligands was performed by nuclear magnetic resonance and by mass spectrometry.

The organothiol-capped Au-NPs were synthesized as described by Brust et al., to produce Au-NPs with a diameter of ∼2 nm.[14] The mole ratio between $HAuCl_4 \cdot 3H_2O$ and the passivating ligands was 1:1. The Au-NPs were rinsed with water in a separatory funnel, concentrated by rotary evaporation, and precipitated in MeOH. The Au-NPs were then stored at 10 °C for 12 h. The Au-NPs were collected by centrifugation, redispersed in toluene, and reprecipitated in MeOH. After 12 h (10 °C), the Au-NPs were recollected by centrifugation and were subsequently vacuum-dried. Table 1 shows the abbreviations of the sensor/ligands studied herein. The NP films were prepared on 1 cm × 2 cm glass substrates that contained metal contacts in the form of a patterned set of interdigitated electrodes (IDEs) consisting of 50 nm of Au deposited over 30 nm of Cr. The electrode pattern produced 20 parallel sets of IDEs, with each IDE having dimensions of 0.240 × 5 mm (width × length), separated by a 10 μm gap. The NP films were cast from a sonicated solution (10 mg mL^{-1} in Tol) by manually depositing a 10 μL drop directly over the region of the substrate that contained the IDEs. The R-SH- and R′-SH-capped Au-NPs were soluble in Tol, whereas poor solubility in Tol was observed for Au-NP's that had the Ar-SH group. Sonication was necessary to increase the Au-NP dispersion. The films were dried under vacuum for 30 min. Thermogravimetric analysis was used to determine the ratio of Au atoms to ligands. For the R-SH-capped Au-NPs, the Au:S-R average mole ratio was 3:1. For the R′-SH-capped Au-NPs, the Au:S-R′ average mole ratio was 3.1:1, whereas for the Ar-SH-capped Au-NPs, the Au:S−Ar average mole ratio was 3.4:1. For the films that contained the C2Ph(Ar) group, the Au:C2Ph mass ratio was 80% Au and 20% C2Ph. Aromatic molecules were added to the solution to produce a sensor film that was composed by mass of 75% Au and 25% organic matrix. Table 2 shows the library of organic vapors, which consisted of six hydrocarbons (A), three polar aprotic vapors (B), and four alcohols (C).

B. Sensing Measurements. An array that contained 20 different types of sensors (two replicates per sensor type) was exposed simultaneously to the test analytes. The sensors were loaded into a rectangular, 40-slot chamber with sensor film replicates positioned randomly. The 45.5 × 3.0 × 1.5 cm (w × l × d) chamber was connected by Teflon tubing to the gas delivery

Table 1. Abbreviations for the Organothiol-Capped Au Nanoparticle Chemical Sensors

R-SH	
1-butanethiol	Au-C4
1-pentanethiol	Au-C5
1-hexanethiol	Au-C6
1-heptanethiol	Au-C7
1-octanethiol	Au-C8
R′-SH	
2-methyl-1-propanethiol	Au-C3(2C)
2-methyl-1-butanethiol	Au-C4(2C)
3-methyl-1-butanethiol	Au-C4(3C)
1-cylohexanethiol	Au-*c*C6
2-ethyl-1-hexanethiol	Au-C6(2C2)
Ar-SH	
1-phenylthiol	Au-Ph
1-naphthalenethiol	Au-Naph
4-biphenylthiol	Au-Biph
2-anthracenethiol	Au-Ant
1,1′,4′,1″-terphenyl-4-thiol	Au-Terph
C2Ph(Ar)[a]	
2-phenylethanethiol	Au-C2Ph
C2Ph, naphthalene	Au-C2Ph(Naph)
C2Ph, biphenyl	Au-C2Ph(Biph)
C2Ph, anthracene	Au-C2Ph(Ant)
C2Ph, terphenyl	Au-C2Ph(Terph)

[a] The C2Ph sensor was composed of functionalized C2Ph Au-NPs, and the C2Ph(Ar) sensors were composed of 25% Ar/C2Ph and 75% Au by mass.

Table 2. Saturated Vapor Pressure, P° (ppm), at 22 °C for All Vapor Analytes Used

	P° ($\times 10^{-4}$)
A	
Hex	17.4
Hept	5.11
Oct	1.54
*i*Oct	5.58
*c*Hex	11.3
Tol	3.17
B	
Chl	22.5
THF	21.3
EtOAc	10.5
C	
MeOH	14.1
EtOH	6.51
*i*POH	4.93
BuOH	0.733

system. The internal cross-sectional area of the chamber was 1 cm^2. The dc resistance of the sensor array was measured with a digital multimeter (Keithley Model 2002) connected to a multiplexing unit (Keithley Model 7001). The resistance data were collected every 5−7 s from the array. A computer-controlled (LabVIEW) flow system delivered pulses of analyte vapor at a given fraction of the analyte's vapor pressure. Oil-free air was obtained from the house compressed air source (1.10 ± 0.15 ppth of water vapor) controlled with a mass flow controller. The total flow rate was 5 L min^{-1} for the duration of the experiment.

The resistance sensitivity of the organothiol-caped Au-NPs sensor films was measured by determining the sensor response as a function of vapor concentration over the concentration range that corresponded to $0.0010 \leq P/P^\circ \leq 0.0200$, where P and P° are the partial pressure and vapor pressure, respectively, of the analyte at room temperature (22 °C), respectively. For the discrimination performance analysis of the sensor arrays, the analyte concentration was maintained at $P/P^\circ = 0.0100$ (22 °C). Each analyte exposure consisted of 70 s of clean laboratory air, 80 s of analyte vapor in air, and 60 s of clean air (to purge the system). A total of 50 exposures per analyte were delivered to the sensor array. The individual exposures were presented in random order. The time required for the 650 total exposures spanned approximately 38 h.

C. Data Preprocessing. All data processing was carried out using MATLAB[26] with custom-written routines. The resistance-based response, r_s, of a vapor sensor to a particular analyte was calculated as $r_s = \Delta R_{max}/R_b$, where R_b is the baseline-corrected resistance of the sensor in the absence of analyte, and ΔR_{max} is the baseline-corrected maximum resistance change upon exposure of the sensor to analyte. A spline was fitted to the baseline data obtained during the pre-exposure period, and values of $\Delta R_{max}/R_b$ were calculated by subtracting the values of the spline, extrapolated over the time of the exposure, from the observed sensor resistance during the exposure period.[13] Prior studies have shown that $\Delta R_{max}/R_b$ is a more reproducible metric than ΔR_{max}.[27,28] The sensitivity of a resistance-based vapor sensor film, s_R, was calculated from the slope of r_s vs P/P°, using a linear least-squares fit.

D. Discrimination Performance. To remove any systematic variation in the data that might be produced by changes in the concentration of analyte produced by the vapor delivery system, prior to analysis, the $\Delta R_{max}/R_b$ responses were sum-normalized:[29]

$$S'_{ij} = \frac{S_{ij}}{\sqrt{\sum_{j=1}^{n} S_{ij}^2}} \quad (1)$$

where S_{ij} is the $\Delta R_{max}/R_b$ sensor response signal of the jth sensor (out of n total sensors) to the ith analyte exposure, and S'_{ij} represents the sum-normalized analog of S_{ij}.

i. Principal Components Analysis. Differences in the sensor response data were visualized using PCA. The normalized data were mean-centered, and diagonalization of the covariance matrix of the data set provided a transformed set of dimensions that best described the data in terms of principal components (PCs). The first PC captured the largest amount of variance in the data; the second PC captured the second most variance in the data (subject to being orthogonal to the first PC), etc. The mean-centered data were then projected onto the first, second, and third PCs, and the data were plotted with respect to these coordinate vectors to observe the natural clustering of the data points. The eigenvalues of the mean-centered covariance matrix provided the relative amounts of variance in each of the corresponding eigenvectors, allowing quantification of the amount of the variance that was captured in the 3-dimensional PC space.

ii. Fisher's Linear Discriminant. FLD was used on the normalized data to evaluate the pairwise discrimination performance of

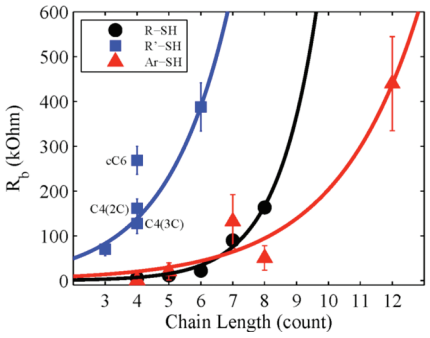

Figure 1. Baseline resistance, R_b (kΩ), obtained from two replicates of each chemiresistive sensor for the R-SH-, R′-SH-, and Ar-SH-capped Au-NP films, as a function of chain length.

the array response between the various test analytes. FLD rotates the *n*-dimensional data space from the exposures to two analytes, and projects an orthogonal vector that maximizes the distance between the average sensor response values. This approach reduces the classification complexity from *n*-dimensions to one dimension. The optimal separation direction is found by maximization of the resolution factor, *rf*:[30]

$$rf = \frac{d}{(\sigma_1^2 + \sigma_2^2)^{1/2}} \quad (2)$$

where d is the distance between the population means, and σ_1 and σ_2 are the standard deviations of the projected populations that correspond to the two analytes of the classification. The *rf* value is similar to a sigma metric; i.e., $rf = 1$ indicates that statistically ∼72% of the data points would be assigned to the correct class of the two possible analytes in the pair; with $rf = 2$, the correct assignment would occur for ∼92% of the data points; whereas with $rf = 3$, the correct assignment would occur statistically for ∼98% of the data points.

Training data were used to determine the projection vector that maximized *rf* and to create a decision boundary for each binary separation task. The decision boundary was a hyperplane normal to the projection vector that assumed a Gaussian clustering of the data. Statistically, points lying on the decision boundary have an equal likelihood of belonging to either of the two clusters. This decision boundary was then used to classify unknown exposures.

The FLD method was applied to all possible pairwise combinations of the 13 analytes tested. The first 25 exposures to each analyte were used to establish the decision boundary. A set of subsequent 25 exposures was then used as unknowns and the test data were classified based on their positions relative to the decision boundary.

III. RESULTS

A. Response Sensitivity. Figure 1 shows the R_b (kΩ) values for the R-SH-, R′-SH-, and Ar-SH-capped Au-NPs chemiresistive films as a function of chain length (i.e., number of carbons). For all of the organothiol-capped Au-NPs, the value of R_b increased as the chain length of the organic ligand increased. Figure S1 (in the Supporting Information) shows the structures of each R′-SH and Ar-SH ligand, with their respective chain length values. Figure 2 shows the s_R values for the organothiol-capped Au-NP sensors upon exposure to the analytes tested. For the R-SH-capped Au-NPs, positive s_R values were observed upon exposure to group A and B vapors, whereas negative s_R values were observed upon exposure to group C vapors. Upon exposure to group A and B vapors, for the R-SH and R′-SH sensors, as the number of carbon atoms in the ligand increased, the value of s_R also increased. Positive values of s_R were observed for the R′-SH sensors upon exposure to group C vapors. The Au-C4(3C) sensor produced very small s_R values upon exposure to group C vapors. In the case of the Ar-SH group, the s_R values obtained upon exposure to the group B and C vapors were higher than those observed upon exposure to the group A vapors. For the A vapors, the Ar-SH-based sensors produced very small values. The C2Ph(Ar) group produced higher s_R values for the group A and B vapors than for the group C vapors. For all of the vapors, considerably lower s_R values were exhibited by the Au-C2Ph-(Naph) and Au-C2Ph(Ant) sensors. Generally, the Au-C2Ph sensor produced the highest s_R values among the Au-C2Ph(Ar) sensor group.

B. Discrimination Performance. *i. Principal Components Analysis.* Figure 3 shows the PCA projection of the first, second, and third principal components of the sum-normalized data. The axes show the fraction of the variance captured by each PC. Figure 3a shows the PC projection of the R-SH-capped Au-NP sensors, showing that the group C vapor clusters were clearly separated from the other vapors, but significant overlap was observed between *i*POH and EtOH. The Chl cluster was well separated from the rest of the vapors. Cluster overlapping was observed between Hex, Hept, Oct, and *i*Oct, as well as overlap between *c*Hex and Tol.

Figure 3b shows the PC projection of the R′-SH-capped Au-NP sensors. All of the group A vapors overlapped, whereas Chl was well separated from the rest of the vapors. The MeOH and EtOH clusters were scattered but fairly well separated from the other vapors, whereas the EtOAc cluster was slightly separated. Figure 3c shows the PC projection observed for the Ar-SH group of sensors. The only well-separated clusters were MeOH and EtOH. Figure 3d shows the PC projection for the C2Ph(Ar) group of sensors. Overlap between all the vapors was observed, and the only minor cluster separation observed was between the THF and Chl vapors.

Figure 3e shows the PC projection for the entire organothiol-capped Au-NP array. The group C vapors were well separated from the group A and B vapors. Overlaps between BuOH and *i*POH, *i*POH and EtOH, and EtOH and MeOH were observed. The group B vapors were separated from the group A and C vapors. For the group A clusters, *c*Hex, *i*Oct, and Tol were separated from Hex, Hept, and Oct, with slight overlaps between Hex and Hept. The Chl, THF, and EtOAc vapor clusters were well separated.

Figure 4 displays the variance that was captured in the first five PCs for the five different types of sensor arrays. For the first PC, the R-SH array captured the highest variance, followed by the R′-SH array. The first PC captured approximately the same variance for the Ar-SH and C2Ph(Ar) sensor arrays. For the second, third, and fourth PCs, the captured variance for the R-SH array was the lowest relative to those obtained for the other sensor arrays. The variance captured by the second, third, and fourth PCs, for the R′-SH, Ar-SH and C2Ph(Ar) sensor arrays, was approximately the same. The values of the variances captured in the first five PCs for an array that contained all of the sensor types were similar to those obtained from the Ar-SH and C2Ph(Ar) arrays.

ii. Fisher's Linear Discriminant. Table S1 (in the Supporting Information) shows the *rf* values for the test analytes with three

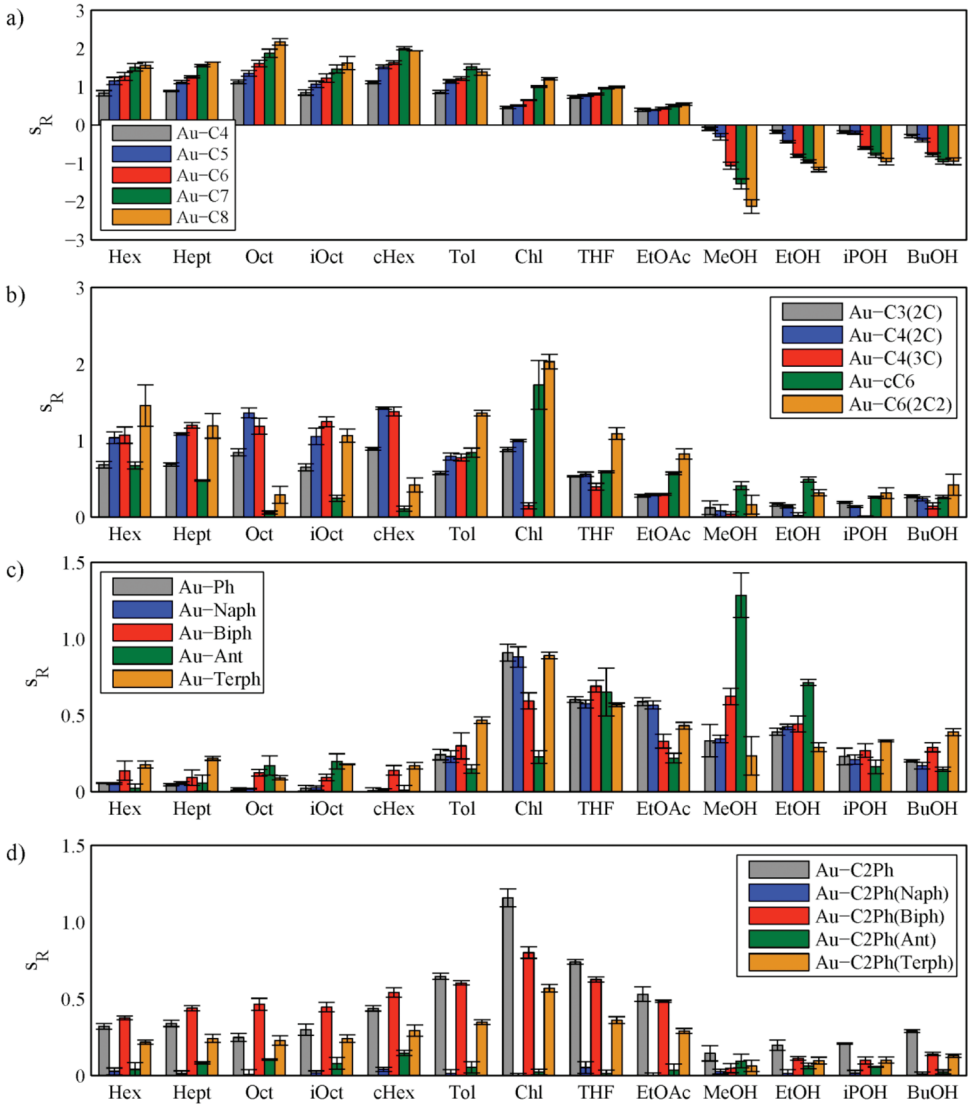

Figure 2. Average resistance-based sensitivities, s_R, for the organothiol-capped Au-NPs exposed to 13 analytes at $0.001 \leq P/P^\circ \leq 0.0200$. Each value is the average of two vapor sensors per sensor type. (a) s_R values for the R-SH-capped Au-NPs sensors, (b) s_R values for the R′-SH-capped Au-NPs sensors, (c) s_R values for the Ar-SH-capped Au-NPs sensors, and (d) s_R values for the C2Ph(Ar) functionalized Au-NPs sensors.

different Au-NP sensor arrays. The respective discrimination performance values are shown in parentheses. A performance value of 1.0 signifies 100% discrimination. Table S1a shows the *rf* values obtained for an array of R-SH-capped Au-NP sensors. The most difficult discrimination tasks (i.e., lower *rf* values) were the binary combinations that included vapors with the same polarity (i.e., nonpolar, polar aprotic, polar protic). Analytes of different polarity were well discriminated. Table S1b shows the *rf* values obtained for an array of R′-SH-capped Au-NP sensors. The binary combinations that included the group B analytes showed the highest *rf* values. Contrary to the R-SH array, the R′-SH array did not produce high *rf* values for binary combinations that included the group C vapors. Table S1c shows the *rf* values obtained for an array of Ar-SH-capped Au-NP sensors. Binary combinations that included *i*Oct and MeOH produced the highest *rf* values. Table S1d shows the *rf* values for an array of C2Ph(Ar) sensors. The highest *rf* values were obtained between vapors that had very different polarities, whereas binary combinations that included vapors within the same polarity group showed the lowest *rf* values. Table S1e shows the *rf* values obtained for an array that contained all of the sensor materials studied. The only binary combination that showed low discrimination was Hept and Oct (*rf* = 1.1).

IV. DISCUSSION

A. Sensor Response Mechanism. The tunneling constant, β_n (carbon^{-1}), for the R-SH-, R′-SH-, and Ar-SH-capped Au-NPs films was determined by using

$$R_b = R_o \exp(n\beta_n) \quad (3)$$

where n is the chain length. The values of β_n were 0.8, 0.5, and 0.4 carbon^{-1}, for the R-SH-, R′-SH-, and Ar-SH-capped Au-NPs, respectively. The response of Au-*c*C6 was excluded in the determination of β_n, due to the deviation of its R_b from the trend exhibited by other ligands, which may reflect the molecular unsaturation of the ligand resulting in a different Au-NP surface passivation as compared to the other R′-SH ligands. The value of β_n obtained

dx.doi.org/10.1021/jp110793h |*J. Phys. Chem. C* 2011, 115, 6208–6217

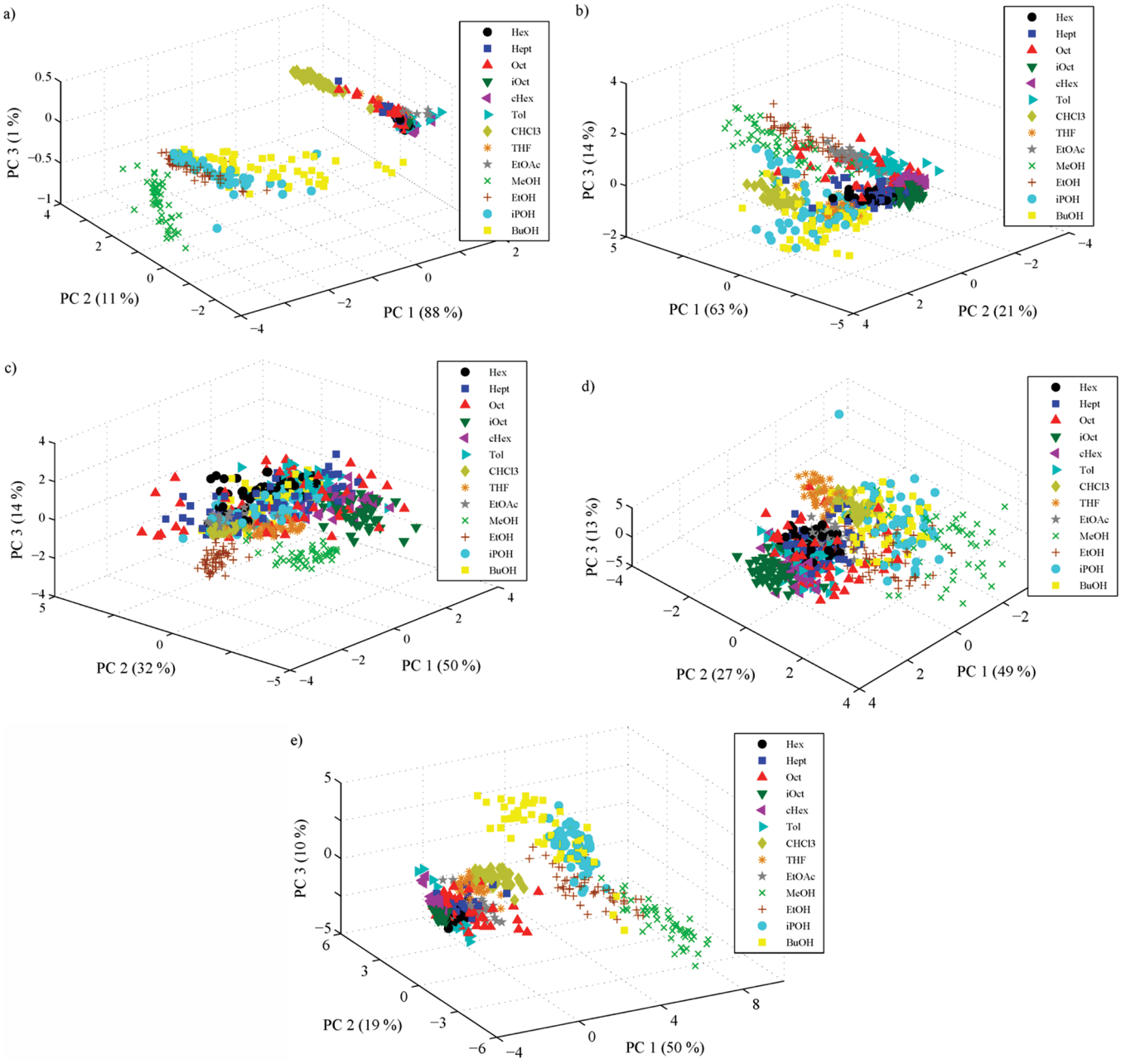

Figure 3. PCA projection of 13 analytes presented to the organothiol-capped Au-NPs at P/P° = 0.0100: (a) projection for a sensor array of R-SH-capped Au-NP sensors (5 sensors total), (b) projection for a sensor array of R′-SH-capped Au-NP sensors (5 sensors total), (c) projection for a sensor array of Ar-SH-capped Au-NP sensors (5 sensors total), (d) projection for a sensor array of CPh2(Ar) functionalized Au-NP sensors (5 sensors total), and (e) projection for a sensor array of all sensor types (20 sensors total).

for R-SH-capped Au-NPs was similar to that determined in previous studies[31] as well as to that determined for aromatic organothiols.[32] The value of β_n for R′-SH-capped Au-NPs was lower than the value of β_n obtained for R-SH-capped Au-NPs. This behavior may reflect the strong hydrophobic interactions of the R′-SH ligands,[33] which could lead to surface voids and thus result in smaller distances between neighboring Au-NPs, thereby increasing the rate of electron hopping between particles in the film.

The R-SH-capped Au-NP sensors showed a characteristic response behavior of exhibiting both positive and negative values of s_R. Conversely, R′-SH did not exhibit such dual response behavior, which could be due to the presence of surface voids that allowed for alcohol vapors to partition into the film. Positive values of s_R were obtained for the reminder of the organothiol-capped Au-NP sensor library. The ligand and/or NPOM organization of the R′-SH, Ar-SH, and C2Ph(Ar) sensors produced a film morphology that allowed alcohol vapors to partition into the sensing film and increase the distance between the Au-NPs (e.g., swelling), unlike the straight-chain alkanethiol-capped Au-NP sensors, where decreases in the distance between Au-NPs upon exposure to alcohol vapors have been observed.[13] Figure S2 (in the Supporting Information) shows the response of a Au-C5 sensor upon exposure to saturated EtOH. The sensor film exhibited an irreversible resistance change that is consistent with an irreversible change in

dx.doi.org/10.1021/jp110793h |J. Phys. Chem. C 2011, 115, 6208–6217

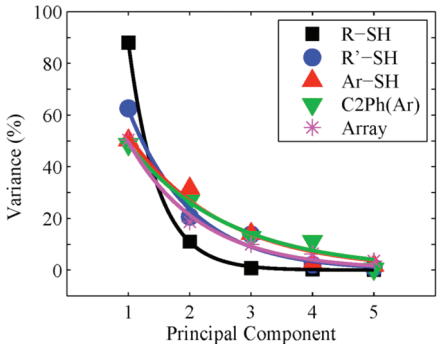

Figure 4. Variance captured as a function of the principal components vector number for five different sensor arrays.

the morphology of the film, in accord with previous observations by SEM for R-SH-capped Au-NPs.[13]

The high selectivity of the Ar-SH group toward group B and C vapors is of note. Polycyclic aromatic compounds pack rigidly on Au surfaces, due to the conjugation of the phenyl rings.[34] The presence of packed molecular islands with different orientations leads to voids on the surface of the Au-NP, which could facilitate the sorption of analyte at the Au-NP surface, as has been observed for flat Au electrodes.[35] Such surface defects could also contribute to low value of β_n. The sorption of polar analytes increases the polarity of the film, facilitating the sorption of more molecules of the same vapor. The low s_R value observed upon exposure to the group A vapors can be attributed to impermeability of the π-stacked system toward nonpolar vapors. In the case of Tol, a high s_R value was obtained due to the permeating aromatic phenyl moiety. The addition of chemical substituents on the terminal Ph ring of the Ar-SH ligands could allow for control over the selectivity of such films. For example, Zhang et al. investigated $CH_3-Ph-SH$ and $OH-Ph-SH$-capped Au-NPs in response to dichloromethane and MeOH. For CH_2Cl_2 vapors, $Ph-CH_3$ produced a higher response than did Ph−OH, whereas for MeOH vapors, OH−Ph produced higher responses than $Ph-CH_3$.[36] For R-COOH and R-NH_2 groups, Johnson et al. observed that $HOOC-Ph-SH$ and $NH_2-Ph-SH$-capped Au-NPs were prone to significant aggregation through hydrogen bond formation.[15] Rowe et al. described the synthesis and electrical properties of 4-mercaptodiphenylacetylene (DPA)-capped Au-NPs. Such DPA-capped Au-NPs demonstrated lower resistances, and thus a higher hopping rate, than R-SH-capped Au-NPs of similar mass.[37] Such ligands could also be chemically modified with different functional groups to control the sensitivity of Au-NPs films.

The difference in the chemical structures of the nonbonding aromatic NPOMs, which were embedded into the C2Ph-capped Au-NP films, produced different s_R values for the various sensors. Low s_R values were observed for Au-C2Ph(Naph) and Au-C2Ph(Ant), whereas high s_R values were observed for Au-C2Ph(Biph) and Au-C2Ph(Terph). The rigid π-stacked formation of Naph and Ant could decrease the availability of vapor sorption sites in the sensor film. Conversely, the rotational single bonds of Biph and Terph allowed for less molecular π-stacking, and allows for more vapor to be sorbed. The influence of the NPOM phase on the s_R values opens a new approach to the development of Au-NP sensor films that can produce a variety of vapor-sensing selectivities, especially for NPOM phases that do not have a coordinating functional group for the Au-NP.

Table 3. Average Resolution Factors, $\overline{rf}$, Obtained from $\Delta R_{max}/R_b$ Values for Each of the Analyte Vapors versus Each Polar Group for Five Different Sensor Arrays: (a) R-SH, (b) R′-SH, (c) Ar-SH, (d) C2Ph(Ar), and (e) All 20 Sensors[a]

	$\overline{rf}$	$\overline{rf}$ vs A	$\overline{rf}$ vs B	$\overline{rf}$ vs C
		(a) R-SH		
Hex	10	0.92	4.0	26
Hept	9.6	0.81	2.4	26
Oct	8.8	1.1	2.2	24
*i*Oct	10	1.2	5.1	26
*c*Hex	11	2.1	5.1	26
Tol	7.9	0.90	2.3	21
Chl	13	6.5	6.0	28
THF	11	2.4	3.8	27
EtOAc	9.8	1.8	3.5	25
MeOH	23	28	32	3.5
EtOH	20	27	26	1.5
*i*POH	23	29	31	1.6
BuOH	12	15	17	2.4
		(b) R′-SH		
Hex	3.4	2.7	4.9	3.2
Hept	2.7	1.4	4.7	2.9
Oct	2.0	1.3	3.1	2.0
*i*Oct	3.7	2.1	5.9	4.1
*c*Hex	3.8	2.0	6.6	3.9
Tol	3.9	3.2	5.6	3.6
Chl	7.1	8.3	8.3	4.6
THF	3.6	3.8	3.8	2.4
EtOAc	4.4	3.4	3.4	3.5
MeOH	3.6	3.9	4.1	2.5
EtOH	3.4	3.5	4.2	2.4
*i*POH	2.5	2.8	2.6	1.8
BuOH	2.8	2.8	3.1	2.5
		(c) Ar-SH		
Hex	1.7	1.6	1.6	1.9
Hept	1.5	1.3	1.6	1.7
Oct	1.1	1.1	1.0	1.1
*i*Oct	4.0	2.1	6.1	4.7
*c*Hex	3.1	1.7	4.2	3.9
Tol	2.9	1.3	4.3	3.9
Chl	3.3	3.5	2.3	3.3
THF	3.0	3.3	2.8	2.7
EtOAc	2.9	2.6	2.6	3.4
MeOH	4.6	4.6	5.6	3.5
EtOH	3.7	3.9	3.6	3.3
*i*POH	1.9	1.9	1.2	2.9
BuOH	1.9	1.2	2.3	2.9
		(d) C2Ph(Ar)		
Hex	3.1	2.2	5.1	2.6
Hept	2.4	1.4	4.4	2.2
Oct	1.7	0.80	2.7	2.2
*i*Oct	4.8	2.5	8.5	4.8
*c*Hex	4.6	1.6	9.6	4.5
Tol	3.0	1.5	5.3	3.2
Chl	6.3	9.0	4.6	3.1

Table 3. Continued

	$\overline{rf}$	$\overline{rf}$ vs A	$\overline{rf}$ vs B	$\overline{rf}$ vs C
THF	4.3	5.6	3.4	2.6
EtOAc	3.1	3.1	4.3	2.4
MeOH	2.5	3.5	2.2	0.97
EtOH	2.2	1.9	3.2	1.8
*i*POH	2.9	4.2	2.5	0.85
BuOH	2.7	3.5	2.8	1.0
		(e) All 20 Sensors		
Hex	11	4.5	7.1	21
Hept	7.0	2.7	4.8	14
Oct	6.4	2.5	4.3	13
*i*Oct	11	3.5	9.7	20
*c*Hex	11	3.9	9.5	20
Tol	6.9	3.7	6.8	11
Chl	12	9.5	12	16
THF	9.9	5.8	6.9	18
EtOAc	9.5	5.8	11	14
MeOH	13	17	14	3.5
EtOH	11	13	13	3.6
*i*POH	18	24	22	2.8
BuOH	11	12	15	3.3

[a] The polar groups were divided into nonpolar vapors (A: Hex, Hept, Oct, *i*Oct, *c*Hex, Tol), polar aprotic vapors (B: Chl, THF, EtOAc), and polar protic vapors (C: MeOH, EtOH, *i*POH, BuOH).

B. Discrimination Performance. *i. Clustering and Overlap Quantification.* FLD can be used to obtain a quantitative measure of the array clustering and overlap, by using the variance captured by the first five PCs. Table S2 (in the Supporting Information) shows the *rf* values and their respective discrimination performance values (parentheses), for each of the sensor arrays, used to produce the PC projections of Figure 3. The *rf* values obtained from the PC projections were generally somewhat higher than the *rf* values displayed in Table S1. This small increase can be attributed to the filtering of response noise using a limited number of PC vectors.

ii. Vapor and Polarity Discrimination Performance. The results obtained in Tables S1 and S2 (in the Supporting Information) can be summarized by averaging the *rf* values obtained for each analyte vs each polar group studied. Table 3 shows the average *rf* values, $\overline{rf}$, for all the binary combinations obtained from the $\Delta R_{max}/R_b$ responses (first column), and the $\overline{rf}$ values obtained vs each vapor group (second to fourth column). For the R-SH group, the highest $\overline{rf}$ values were obtained for the group C vapors, due to the negative sign of the $\Delta R_{max}/R_b$ response values. Vapor misclassification was obtained when the binary combination contained analytes within the same vapor group. For group C vapors, as the carbon chain became longer, the $\overline{rf}$ became lower due to an increase of the proportion of nonpolar moiety. The R′-SH group produced discrimination $\overline{rf}$ values for most of the binary combinations, except for the combinations that contained vapors within the same polarity group, such as the A and C groups. The $\overline{rf}$ values obtained for the binary combinations within the A group were higher than those produced by the R-SH array. The higher $\overline{rf}$ values were obtained for the group B vapors. The R-SH produced higher overall $\overline{rf}$ values than the R′-SH group. Conversely, for binary combinations of analytes within the same polarity group, the R′-SH group performed better. The Ar-SH group, in comparison with the other sensor groups, produced the highest $\overline{rf}$ values for vapors within the C group. In the case of the C2Ph(Ar) group, the highest discrimination $\overline{rf}$ values were obtained for the group B vapors.

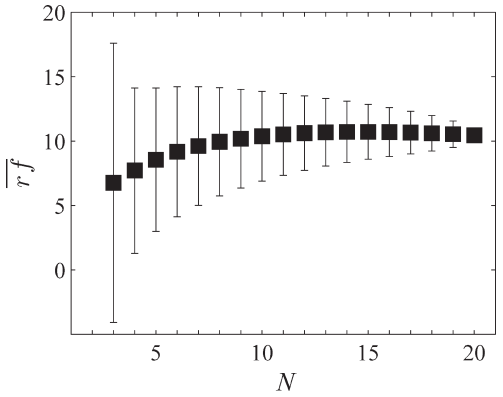

Figure 5. Average resolution factor values $\overline{rf}$ as a function of array size (i.e., number of sensors), *N*. Each $\overline{rf}$ value represents the average of all binary combinations of analytes, for all possible array sizes in each system.

Table 3e shows the $\overline{rf}$ values produced for an array that contained of all the sensor types. Vapor discrimination $\overline{rf}$ values were obtained for all combinations except for the combinations of Oct vs group A vapors and *i*POH vs group C vapors. Table S3 (in the Supporting Information) shows the $\overline{rf}$ values obtained from the *rf* values obtained in Table S2. The $\overline{rf}$ values showed the same patterns observed in Table 3, albeit their magnitude was higher due to the filtering of response noise using a limited number of PC vectors.

iii. Discrimination Performance Dependence on Sensor Array Size and Sensitivity. The magnitude of the *rf* values obtained in Table 3e was also influenced by the array size.[38] The total number of combinations, *C*, per array size, *N*, is given by

$$C = \frac{N_{Total}!}{N!(N_{Total} - N)!} \quad (4)$$

where N_{Total} is the total number of sensors ($N_{Total} = 20$), and *r* is the array size (i.e., number of sensors in array). Figure 5 shows the average *rf* values, $\overline{rf}$, for all possible combinations of sensors for each possible array size. As the value of *N* increased, the $\overline{rf}$ value also increased. Arrays of two sensors are not displayed due to high standard deviations and low values of recognition, as observed by Park et al.[39] The maximum $\overline{rf}$ value was obtained for $N \geq 13$ sensors. The larger number of sensors is beneficial for resolving, on average, a generalized set of test vapors. A larger number of sensors and descriptors increases the probability that the dimensionality of vapor space is fully spanned by the array.[40,41]

The value of s_R for each sensor in the array, and the average sensitivity, $\overline{s_R}$, of the array could influence the discrimination performance. Figure 6 shows the $\overline{rf}$ values obtained for all possible arrays for $N = 4$, 10, and 19 sensors, as a function of $\overline{s_R}$, for each possible array of a given *N*. A linear least-squares fit has also been depicted. For $N = 4$ and 10 sensors, as the $\overline{s_R}$ increased, the value of $\overline{rf}$ also increased. Conversely, for $N = 19$ sensors, as the average s_R increased, the value of $\overline{rf}$ decreased. Figure 7 shows the slope, ζ, obtained from linear least-squares fit (i.e., red line) depicted in Figure 6 as function of *N*. The magnitude of the slope increased from $N = 3$ to 4; however, the value decreased until reaching an inflection point at ~10 sensors. For $N = 13$ sensors, the value of the slope was ~0, becoming negative for $N > 13$ sensors. The 0 value of ζ for $N = 13$

dx.doi.org/10.1021/jp110793h |*J. Phys. Chem. C* 2011, 115, 6208–6217

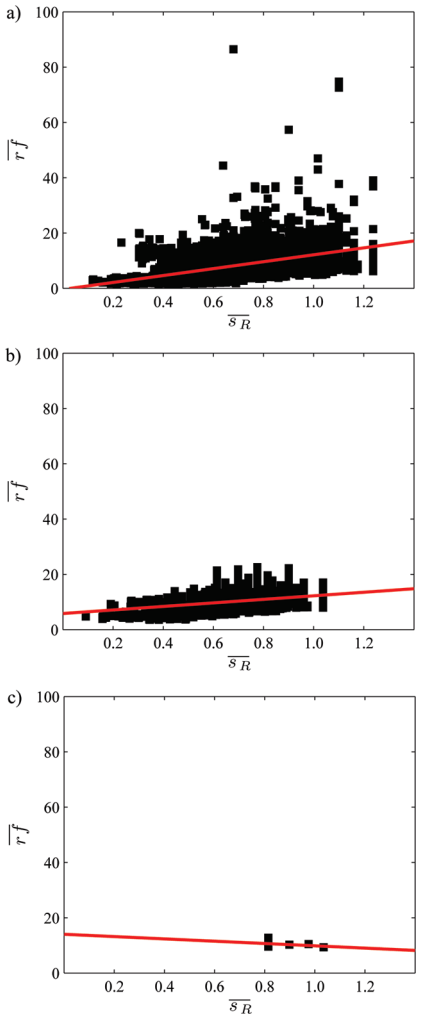

Figure 6. Average resolution factor, $\overline{rf}$, as a function of the average resistance sensitivity, $\overline{s_R}$, for all possible arrays for three different values of N, (a) $N = 4$ sensors, (b) $N = 10$ sensors, and (c) $N = 19$ sensors. Each square represents the average $\overline{rf}$ value for an array with an average $\overline{s_R}$. The red line represents the linear least-squares fit.

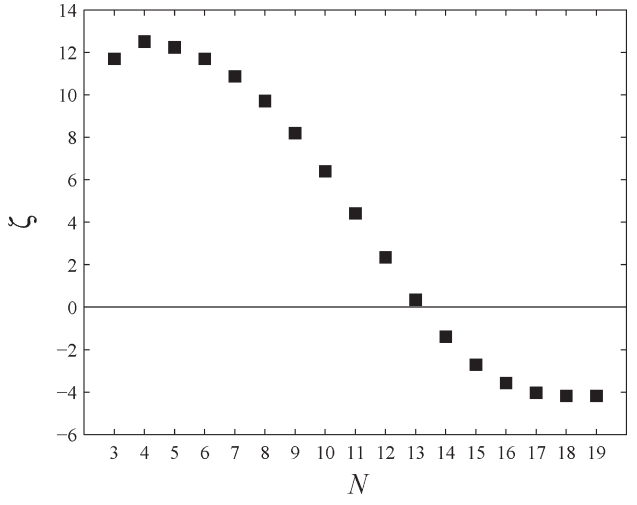

Figure 7. Slope, ζ, as a function of the array size (i.e., number of sensors), n.

confirmed that approximately the maximum discrimination performance of an array of organothiol-capped Au-NPs was reached at such N, as observed in Figure 5.

V. CONCLUSIONS

The vapor selectivity, as determined by the resistance response sensitivity, of an array of organothiol-capped Au-NPs is well described by considering the polarity of the vapor and the passivating ligand, as well as the chemical structure of the passivating ligand. For straight-chain alkanethiol-capped Au-NPs, a dual response mechanism was observed, in which positive $\Delta R_{max}/R_b$ values were obtained upon exposure to hydrocarbons and polar analytes, whereas negative $\Delta R_{max}/R_b$ values were obtained upon exposure to alcohols. The value of $|s_R|$ increased as the length of the alkanethiol increased. Branched alkanethiol-capped Au-NPs did not shown a dual response mechanism, perhaps due to surface defects, but their responses followed a monotonic chain length trend (except of Au-*c*Hex), in which a higher number of carbons in the ligand produced higher values of $|s_R|$. Functionalized Au-NPs with aromatic thiols showed high selectivity toward polar vapors, due to the presence of molecular π-stacked islands on the surface of the NP, which allowed for voids to sorb polar analytes. The incorporation of NPOMs in the organothiol-capped Au-NP films allowed for control at the molecular level over the selectivity of the sensor film.

The dual response mechanism for the alkanethiol-capped Au-NPs detectors produced better discrimination performance for group C vapor responses, but misclassified vapors that contained a mutually similar functionality. In contrast, a R′-SH-containing sensor array was able to discriminate vapors that had a mutually similar chemical functionality. The Ar-SH group classified alcohol vapors better than did the other arrays, whereas the C2Ph(Ar) sensor array classified aprotic polar vapors better than did the other arrays. A sensor array that consisted of 20 different organothiol-capped Au-NPs exhibited a 100% discrimination between 13 test organic vapors at a partial pressure of $P/P^\circ = 0.0100$. Maximum classification for an array of organothiol-capped Au-NPs was achieved for an array size of 13 or more sensors.

■ ASSOCIATED CONTENT

Supporting Information. Table S1 shows resolution factors, rf, and performance values (parentheses) for all possible binary combinations of analytes tested at $P/P^\circ = 0.0100$ by using the $\Delta R_{max}/R_b$ values. Table S2 shows resolution factors, rf, and performance values (parentheses) for all possible binary combinations of analytes tested at $P/P^\circ = 0.0100$ by using the by the variance of the first five PCs. Table S3 shows resolution factor averages, $\overline{rf}$, obtained by the first five principal components from the variances captured, for each of the analyte vapors versus each polar group, for five different sensor arrays. Figure S1 shows the molecular structures and the chain length determination for all ligands. Figure S2 shows the response of a Au-C5 sensor upon exposure to saturated ethanol. This material is available free of charge via the Internet at http://pubs.acs.org.

■ AUTHOR INFORMATION

Corresponding Author

*Phone: 626-395-6335. Fax: 626-395-8867. E-mail: nslewis@caltech.edu.

■ ACKNOWLEDGMENT

T.G. acknowledges the support from Tyco Electronics Corp. Research was carried out in the Molecular Materials Research Center of the Beckman Institute at Caltech. This work was supported by the NSF and by DHS. NSF is acknowledged for a graduate fellowship to E.G.-B..

■ REFERENCES

(1) Burns, J. A.; Whitesides, G. M. *Chem. Rev.* **1993**, *93*, 2583.
(2) Duda, R. O.; Hart, P. E. *Pattern Classification and Scene Analysis*; John Wiley & Sons: New York, 1973.
(3) Geladi, P.; Kowalski, B. R. *Anal. Chim. Acta* **1986**, *185*, 1.
(4) Kowalski, B. R.; Bender, C. F. *Anal. Chem.* **1972**, *44*, 1405.
(5) Gao, T.; Woodka, M. D.; Brunschwig, B. S.; Lewis, N. S. *Chem. Mater.* **2006**, *18*, 5193.
(6) Maldonado, S.; Garcia-Berrios, E.; Woodka, M. D.; Brunschwig, B. S.; Lewis, N. S. *Sens. Actuators, B* **2008**, *134*, 521.
(7) Woodka, M. D.; Brunschwig, B. S.; Lewis, N. S. *Langmuir* **2007**, *23*, 13232.
(8) Freund, M. S.; Lewis, N. S. *Proc. Natl. Acad. Sci. U.S.A.* **1995**, *92*, 2652.
(9) Severin, E. J.; Doleman, B. J.; Lewis, N. S. *Anal. Chem.* **2000**, *72*, 658.
(10) Pearson, R. G. *J. Am. Chem. Soc.* **1963**, *85*, 3533.
(11) Sellers, H.; Ulman, A.; Shnidman, Y.; Eilers, J. E. *J. Am. Chem. Soc.* **1993**, *115*, 9389.
(12) Wohltjen, H.; Snow, A. W. *Anal. Chem.* **1998**, *70*, 2856.
(13) García-Berríos, E.; Gao, T.; Maldonado, S.; Woodka, M. D.; Ellsworth, M. W.; Brunschwig, B. S.; Lewis, N. S. *J. Phys. Chem. C* **2010**, *114*, 21914.
(14) Brust, M.; Walker, M.; Bethell, D.; Schiffrin, D. J.; Whyman, R. J. *J. Chem. Soc., Chem. Commun.* **1994**, 801.
(15) Johnson, S. R.; Evans, S. D.; Brydson, R. *Langmuir* **1998**, *14*, 6639.
(16) Woehrle, G. H.; Brown, L. O.; Hutchison, J. E. *J. Am. Chem. Soc.* **2005**, *127*, 2172.
(17) Guo, J. L.; Pang, P. F.; Cai, Q. Y. *Sens. Actuators, B* **2007**, *120*, 521.
(18) Han, L.; Daniel, D. R.; Maye, M. M.; Zhong, C. J. *Anal. Chem.* **2001**, *73*, 4441.
(19) Ibañez, F. J.; Zamborini, F. P. *ACS Nano* 2008.
(20) Han, L.; Shi, X. J.; Wu, W.; Kirk, F. L.; Luo, J.; Wang, L. Y.; Mott, D.; Cousineau, L.; Lim, S. I. I.; Lu, S.; Zhong, C. J. *Sens. Actuators, B* **2005**, *106*, 431.
(21) Wang, L. Y.; Kariuki, N. N.; Schadt, M.; Mott, D.; Luo, J.; Zhong, C. J.; Shi, X. J.; Zhang, C.; Hao, W. B.; Lu, S.; Kim, N.; Wang, J. Q. *Sensors* **2006**, *6*, 667.
(22) Wang, L. Y.; Shi, X. J.; Kariuki, N. N.; Schadt, M.; Wang, G. R.; Rendeng, Q.; Choi, J.; Luo, J.; Lu, S.; Zhong, C. J. *J. Am. Chem. Soc.* **2007**, *129*, 2161.
(23) Marvel, C. S.; Caesar, P. D. *J. Am. Chem. Soc.* **1950**, *72*, 1033.
(24) Koval, I. V. *Usp. Khim.* **1993**, *62*, 813.
(25) Field, L.; Grunwald, F. A. *J. Org. Chem.* **1951**, *16*, 946.
(26) MathWorks, T. MATLAB R2010b, 2010.
(27) Briglin, S. M.; Gao, T.; Lewis, N. S. *Langmuir* **2004**, *20*, 299.
(28) Sisk, B. C.; Lewis, N. S. *Sens. Actuators, B* **2003**, *96*, 268.
(29) Otto, M. *Statistics and Computer Application in Analytical Chemistry*; Wiley-VCH: New York, 1999.
(30) Brereton, R. G. *Data Analysis for the Laboratory and Chemical Plant*; John Wiley & Sons: West Sussex, England, 2003.
(31) Zamborini, F. P.; Leopold, M. C.; Hicks, J. F.; Kulesza, P. J.; Malik, M. A.; Murray, R. W. *J. Am. Chem. Soc.* **2002**, *124*, 8958.
(32) Rampi, M. A.; Whitesides, G. M. *Chem. Phys.* **2002**, *281*, 373.
(33) Chi, Q. J.; Zhang, J. D.; Ulstrup, J. *J. Phys. Chem. B* **2006**, *110*, 1102.
(34) Frey, S.; Stadler, V.; Heister, K.; Eck, W.; Zharnikov, M.; Grunze, M.; Zeysing, B.; Terfort, A. *Langmuir* **2001**, *17*, 2408.
(35) Scharf, J.; Strehblow, H. H.; Zeysing, B.; Terfort, A. *J. Solid State Electrochem.* **2001**, *5*, 396.
(36) Zhang, H. L.; Evans, S. D.; Henderson, J. R.; Miles, R. E.; Shen, T. H. *Nanotechnology* **2002**, *13*, 439.
(37) Rowe, M. P.; Plass, K. E.; Kim, K.; Kurdak, C.; Zellers, E. T.; Matzger, A. J. *Chem. Mater.* **2004**, *16*, 3513.
(38) Burl, M. C.; Sisk, B. C.; Vaid, T. P.; Lewis, N. S. *Sens. Actuators, B* **2002**, *87*, 130.
(39) Park, J.; Groves, W. A.; Zellers, E. T. *Anal. Chem.* **1999**, *71*, 3877.
(40) Doleman, B. J.; Severin, E. J.; Lewis, N. S. "Method of Resolving Analytes in a Fluid"; G01N 033/497 G01N 033/48 ed.; U.S. Patent; California Institute of Technology, Pasadena, CA, 1999; pp 1.
(41) Lewis, N. S.; Severin, E. J.; Freund, M.; Matzger, A. J. "Use of an Array of Polymeric Sensors of Varying Thickness for Detecting Analytes in Fluids"; U.S. Patent; California Institute of Technology, Pasadena, CA, 2004; pp 1.

■ NOTE ADDED AFTER ASAP PUBLICATION

This article was published ASAP on March 15, 2011. Figures 5, 6, and 7 and their captions have been modified. The correct version was published on March 21, 2011.